Monthly Notices
of the
ROYAL ASTRONOMICAL SOCIETY

MNRAS **451,** 3061–3067 (2015) doi:10.1093/mnras/stv1134

Effects of the variability of the nucleus of NGC 1275 on X-ray observations of the surrounding intracluster medium

A. C. Fabian,[1]⋆ S. A. Walker,[1] C. Pinto,[1] H. R. Russell[1] and A. C. Edge[2]

[1]*Institute of Astronomy, Madingley Road, Cambridge CB3 0HA, UK*
[2]*Department of Physics, Durham University, Durham DH1 3LE, UK*

Accepted 2015 May 13. Received 2015 May 11; in original form 2015 April 15

ABSTRACT

The active galaxy NGC 1275 lies at the centre of the Perseus cluster of galaxies, which is the X-ray brightest cluster in the Sky. The nucleus shows large variability over the past few decades. We compile a light curve of its X-ray emission covering about 40 years and show that the bright phase around 1980 explains why the inner X-ray bubbles were not seen in the images taken with the *Einstein* Observatory. The flux had dropped considerably by 1992 when images with the *ROSAT* HRI led to their discovery. The nucleus is showing a slow X-ray rise since the first *Chandra* images in 2000. If it brightens back to the pre-1990 level, then X-ray absorption spectroscopy by *ASTRO-H* can reveal the velocity structure of the shocked gas surrounding the inner bubbles.

Key words: galaxies: active – galaxies: clusters: individual: Perseus – galaxies: individual: NGC 1275.

1 INTRODUCTION

The Perseus cluster of galaxies, the X-ray brightest cluster in the Sky, has an X-ray cool core surrounding the active central galaxy NGC 1275. The jets forming its radio source 3C 84 blow 15 kpc diameter bubbles in the hot gas (Boehringer et al. 1993; Fabian et al. 2000, 2006). Buoyant ghost bubbles lie further from the nucleus, revealing the last 10^8 yr or more of energy feedback from the AGN to the cool core.

Radio and γ-ray light curves of the active nucleus of NGC 1275 show large amplitude variability over the past 40 years (Abdo et al. 2009; Dutson et al. 2014). The source was bright from the 1960s to about 1990 when it abruptly faded by about an order of magnitude. It was faintest around 2000 and now shows signs of increasing again.

Here, we look at the long-term variability of NGC 1275, finding it to have dropped by about a factor or 20 between when first imaged with the *Einstein* Observatory in 1980 and *Chandra* in 2000, rising slowly since then. We demonstrate that the high brightness of the nucleus prevented detection of the inner bubbles with the *Einstein* Observatory in the (relatively) short exposure times used.

We also examine the possibility of detecting resonance line absorption from the hot gas using the nucleus as a backlight. It appears that if the nucleus remains at the 2006 level or similar then such absorption would be challenging with *ASTRO-H*, due to its half energy width of 1.5 arcmin causing the nucleus to appear at low contrast against the bright hot gas emission. It will be straightforward for *Athena* with its angular resolution of 5 arcsec or better. If, however, the nucleus increases to the 1980 level, then it will compromise emission line studies of the central region with *ASTRO-H*, but make absorption spectroscopy possible. Since our line of sight passes directly through the shocked gas surrounding the 1100 km s^{-1} expanding southern bubble, such studies would give unique insight and test the growth and energetics of the bubbles.

2 OBSERVATIONS

We investigate the variation in X-ray flux from the central AGN in Perseus by analysing all of the spatially resolved X-ray observations that have been taken of the system, starting with the first *Einstein* observation from 1979. The observations used are listed in Table 1. In addition we have compiled a comprehensive list of hard energy spectral measurements for NGC 1275 from *Copernicus*, OSO-7, *HEAO*-1 A-4, *EXOSAT* LE, *Ginga* LAC, OSSE and several balloon experiments (Table 1). Full width at half-maximum (FWHM) for the imaging instruments is tabulated. The early *Copernicus* estimate contains an uncertain level of cluster emission so is shown as an upper limit.

From the cleaned events files we find the count rate within a circular region centred on the AGN of diameter equal to the FWHM for the instrument used. The count rate was then converted into the 0.5–10.0 keV flux using WebPimms, under the assumption that the spectrum of the AGN is a power law of index 1.65, as was found in the *XMM–Newton* study of Churazov et al. (2003). Residual cluster

⋆ E-mail: acf@ast.cam.ac.uk

Table 1. Archival Perseus cluster observations.

Telescope	Detector	FWHM (arcsec)	Obs ID	Year	Day	Exposure (ks)	Reference
Copernicus		120		1972 September			Fabian et al. (1974)
UCSD OSO-7				1972 November 9–27			Rothschild et al. (1981)
HEAO-1 A4				1977 August; February, 1978 August			Primini et al. (1981)
Einstein	HRI	3	h0316n41.xia	1979	52	15.6	Fabian et al. (1981)
Einstein	HRI		h0316n41.xib	1980	49	6.6	Fabian et al. (1981)
TESRE Balloon				1981 September 29			Matt et al. (1990)
EXOSAT	LE LX3	15	ex830724	1983	205	13.4	Allen et al. (1992)
EXOSAT	LE LX3		ex840124	1984	24	2.3	Allen et al. (1992)
SPARTAN-1				1984 August			Ulmer et al. (1987)
SPACELAB-2				1985 September			Eyles et al. (1991)
Ginga				1989	15–17		Allen et al. (1992)
OSSE				1991 November 28 -12 December 12			Osako et al. (1994)
ROSAT	HRI	2	rh800068n00	1991	41	10.9	Boehringer et al. (1993)
ROSAT	HRI		rh800591a01	1994	217	52.9	
ROSAT	HRI		rh702626n00	1996	42	8.2	
ROSAT	HRI		rh702626a01	1997	62	4.6	
XMM	PN	7	P0085110101PN	2001	30	51.2	Churazov et al. (2003)
XMM	PN		P0305780101PN	2006	29	119	
Swift	XRT	7	sw00036524002xpcw2po	2007	340	3.6	
Swift	XRT		sw00030354003xpcw3po	2009	364	4.3	
Swift	XRT		sw00031770009xpcw3po	2010	219	2.1	
Swift	XRT		sw00049799006xpcw3po	2013	213	1.6	

Notes. *Copernicus*: 12, 6, and 2 arcmin apertures; OSO-7: 6.5 deg FWHM; *HEAO*-1: 1.7 × 20 deg; *TESRE balloon*: 3 deg; *SPARTAN*-1: 5 arcmin × 3 deg; *SPACELAB*-2: 12 arcmin; *Ginga*: 0.8 × 1.7 deg; *OSSE*: 3.8 × 11.4 deg.

emission is unlikely to contribute significantly to the measured nucleus flux when it is bright.

The resulting X-ray light curve is shown in Fig. 1, with points from different missions labelled and shown with different colours. The X-ray light curve shows a decrease by nearly an order of magnitude from the early 1980s to the 1990s. This is in good agreement with the decrease observed in the 90-GHz radio emission reported in Dutson et al. (2014), which is plotted as the grey points.

3 SIMULATED *EINSTEIN* IMAGES

The *Einstein* Observatory's HRI instrument observed the Perseus cluster for 15.6 ks in 1979 February, and again for 6.6 ks in 1980 February. The central cavities cannot be resolved in either of these images, even when they are stacked together.[1] The cavities remained undiscovered until the first *ROSAT* HRI observations of Perseus (Boehringer et al. 1993), which showed for the first time clear evidence for the interaction between the relativistic particles in the radio lobes and the intracluster medium (Fig. 2).

The on axis spatial resolution of the *Einstein* HRI was, however, comparable to that of the *ROSAT* HRI (3 arcsec FWHM for *Einstein*, 2 arcsec FWHM for *ROSAT*). It is therefore interesting to see whether the high X-ray flux from the central AGN during the *Einstein* mission prevented *Einstein* from making the first detection of the cavities in Perseus.

We therefore simulated *Einstein* images of Perseus to investigate the visibility of the central cavities as a function of the central AGN flux and exposure time. The simulations were performed using SIMX,[2] which was modified to allow it to simulate the *Einstein* observatory. This was achieved by setting the focal length, field of view and pixel size parameters equal to those for the *Einstein* HRI, and using *Einstein* RMF and ARF response files. The PSF was set by using the Encircled Energy Function from Van Speybroeck (1979). For the input image we used the stacked, 890 ks, *Chandra* image from Fabian et al. (2006). Since only one spectrum can be used when simulating an events file with SIMX, we simulated separate events files for the central AGN and the cluster emission with different spectra for each, and then added them. For the central AGN the input spectrum was set as a powerlaw of index 1.65, as found in Churazov et al. (2003). For the cluster emission the input spectrum was a thermal APEC component with parameters fixed to the mean cluster temperature in the core ($kT = 4$ keV).

We perform *Einstein* HRI simulations with three different AGN flux levels and three different exposure times, and these are shown in Fig. 3. The top row in Fig. 3 shows simulations using the 1979 AGN flux level (7.3×10^{-11} erg s^{-1} cm^{-2} in the 0.5–10keV band) for exposure times of 1 × , 10 × and 100 × that of the 15.6 ks *Einstein* observation from 1979. With the AGN at its 1979 flux level, the PSF spreading prevents the central cavities from being robustly measured even in very deep (1.5 Ms) observations. The north western 'ghost' cavity is however resolved in the ≥156 ks simulations.

The second row shows the case when the central AGN flux is reduced to its minimum observed level (from around 2002) of 5×10^{-12} erg s^{-1} cm^{-2} in the 0.5–10 keV band. We see that a 15.6 ks observation can begin to resolve the inner cavities (first column, 2nd row in Fig. 3). With ten times this exposure time, the cavity system is clearly resolved, showing a similar level of detail as the *ROSAT* HRI observations.

[1] A decrease in X-ray emission at the position of the NW ghost cavity is apparent in the *Einstein* image, and was commented on at the time (Branduardi-Raymont et al. 1981; Fabian et al. 1981). Since it is devoid of detected radio emission, its true nature was unsuspected.

[2] http://hea-www.cfa.harvard.edu/simx/

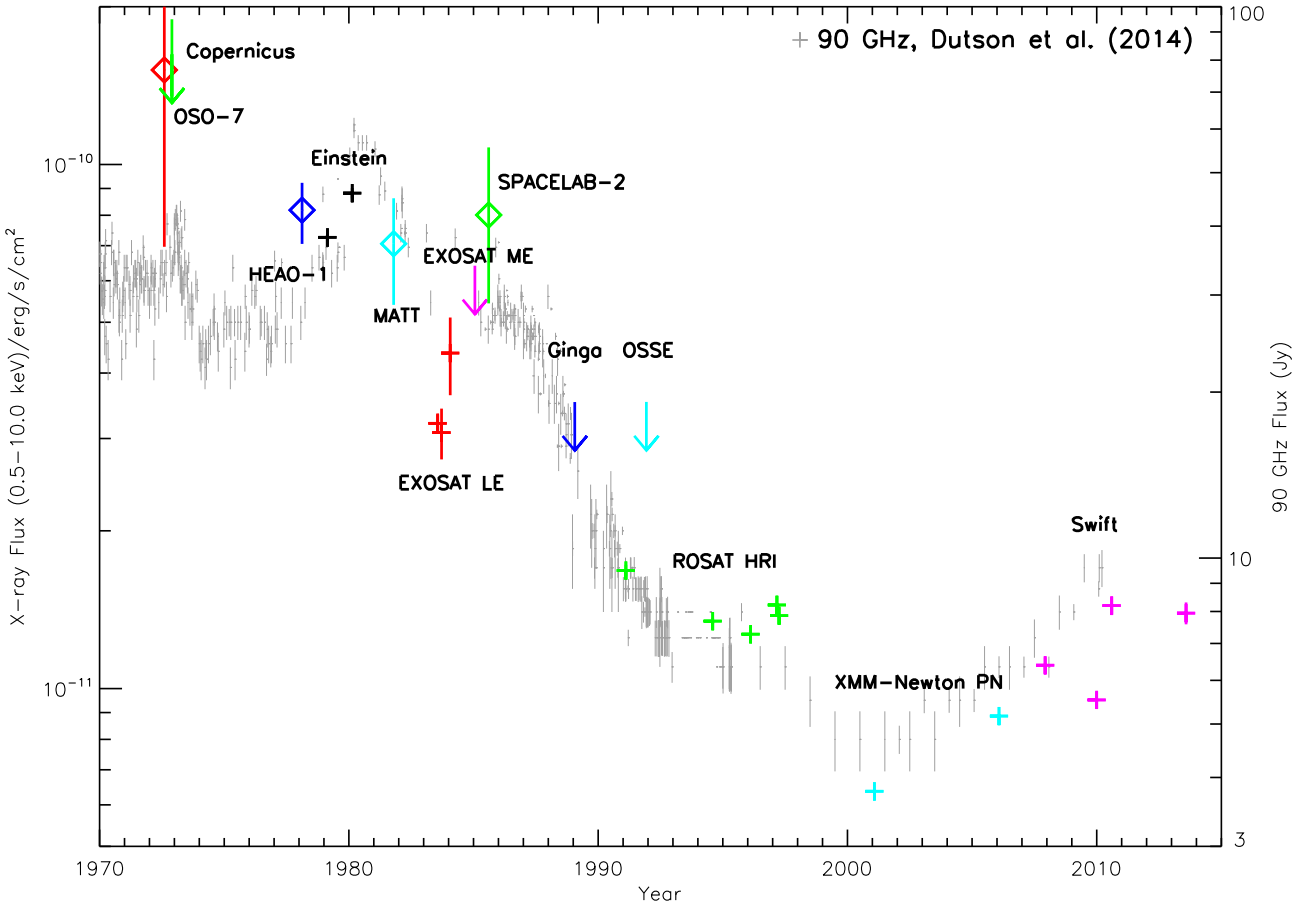

Figure 1. Variation in X-ray flux from the central AGN in Perseus from the 1970s to the present day. The grey points show the 90-GHz radio light curve gathered by Dutson et al. (2014), which follows a similar trend to the X-ray light curve.

Finally, in the third row, we show a simulated *Einstein* image of the case where there is no contribution from a central AGN (bottom row), allowing us to demonstrate *Einstein's* ability to resolve fluctuations in extended X-ray emission from the intracluster medium (ICM) in the idealized case of no point source contamination. We see that even in a 15.6 ks observation, matching the exposure time of the 1979 *Einstein* observation, the inner cavities can just about be resolved. Structure is seen on the scale of the radio source which may at least have triggered further observation. The cavity system is comfortably resolved with an exposure time which is ten times deeper.

4 X-RAY ABSORPTION SPECTROSCOPY USING NGC 1275

In this section, we analyse absorption by the ICM acting on the AGN emission, using a multiphase collisionally-ionized absorber. To calculate the column density of gas in each temperature range, we extracted azimuthally averaged temperature and density profiles from the *Chandra* data, which were deprojected using the DSDEPROJ direct spectral deprojection method (Sanders & Fabian 2007; Russell, Sanders & Fabian 2008). The reduction of the *Chandra* data is described in Sanders & Fabian (2007). We integrated the deprojected density profile along the line of sight to find the column density in the following temperature bands which are tabulated in Table 2; <2, 2–3, 3–4, 4–5 and 5–6 keV.

The lowest two temperature components are associated with the high pressure (shocked) rims around the bubbles (Fig. 6). The density jump at the outer edge of the rims is 1.3 and the inferred Mach number is 1.2 (Graham, Fabian & Sanders 2008).

For the absorption, each phase was modelled with a single-temperature *hot* model in SPEX[3] (version 2.03.03), which calculates the transmission of a collisionally-ionized equilibrium plasma. For a given temperature and set of abundances, the model calculates the ionization balance and then determines all the ionic column densities by scaling to the prescribed total hydrogen column density. We used five *hot* components with temperatures and hydrogen column densities as quoted in Table 2. We adopted a metallicity of 0.65 (Sanders & Fabian 2007) and a nominal velocity dispersion of 300 km s^{-1} We show the transmission of this multitemperature absorber near the Fe K complex in Fig. 4 with the strongest absorption line labelled. An AGN spectrum provided with both high spatial and spectral resolution would reveal a strong absorption feature at 6.58 keV.

In order to estimate the nuclear emission of NGC 1275, we have analysed the longest on-axis exposure of the Perseus cluster taken with *XMM-Newton*/EPIC in 2006 (ID=0305780101). Data were reduced and corrected by solar flares with the *SAS* v14 following the standard *XMM–SAS* procedure. We extracted the nuclear spectrum and subtracted the cluster spectrum following the procedure of

[3] www.sron.nl/spex

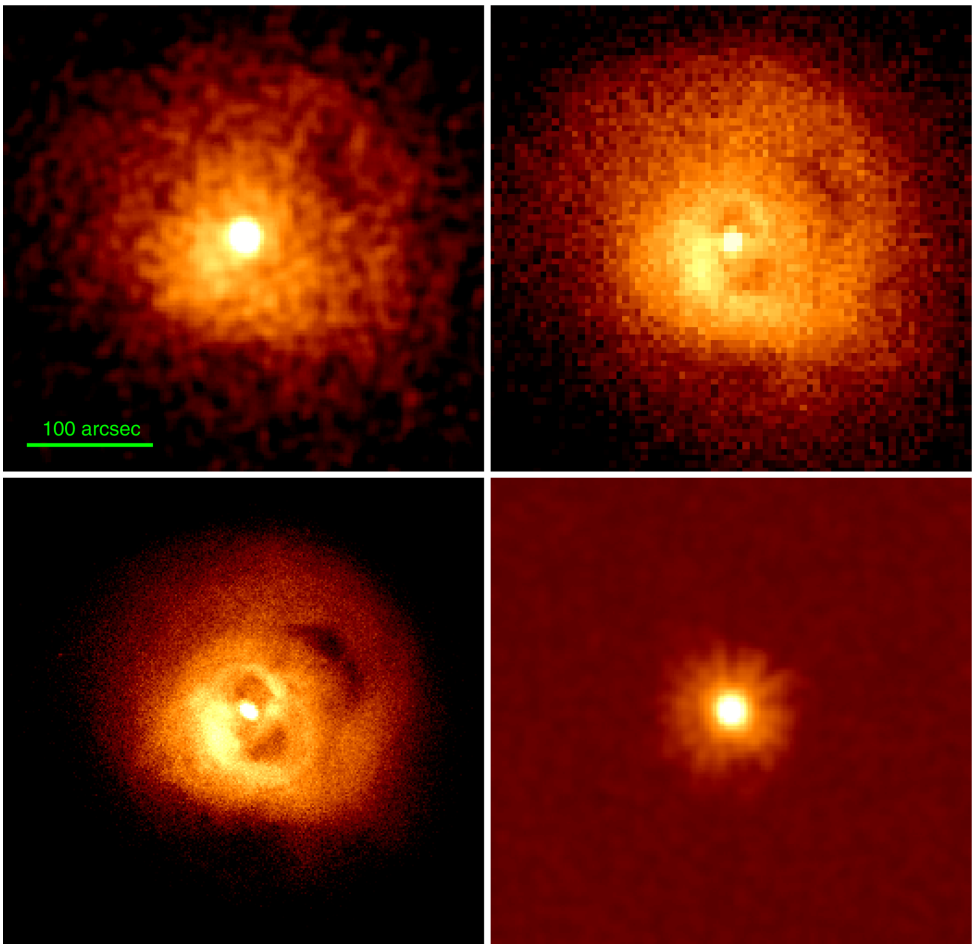

Figure 2. Clockwise from top left: *Einstein* HRI image of NGC 1275; *ROSAT* HRI image of NGC 1275; *Einstein* HRI image of the bright quasar 3C 273 to same angular scale; *Chandra* image of NGC 1275. The *Einstein* image has been lightly smoothed.

Churazov et al. (2003). The cluster-subtracted nucleus spectrum was then fitted with a power law and a Gaussian to model the nuclear Fe K emission line, both redshifted and absorbed by the Galactic foreground. EPIC spectra do not have spectral resolution high enough to resolve any narrow absorption lines of the foreground ICM.

The X-ray integral field unit (X-IFU) aboard *Athena* is planned to have spatial (5 arcsec) and spectral (2.5 eV) resolution at 6 keV high enough to resolve the Fe K lines absorbed by the nucleus. We used the nuclear spectral model fitted with the EPIC spectra as a template model to simulate a 100 ks X-IFU spectrum. On top of the AGN emission the multiphase absorber was tested with three different values of velocity dispersion v_σ (see Fig. 5. The high-quality X-IFU spectrum will easily resolve the lines.

The *ASTRO-H* Soft X-ray Spectrometer (SXS) with its 5 eV spectral resolution could potentially resolve absorption in the nucleus emission of NGC 1275, but due to the large 1.5 arcmin HEW, the SXS central chip will include both the central AGN and the cluster emission from a region of about 1.5 arcmin width. In order to estimate the cluster emission, we extracted a further EPIC spectrum in an annulus of 0.75 arcmin outer radius and inner radius equal to that of the nuclear region (14 arcsec, see Churazov et al. 2003). We modelled the cluster spectrum with a 4 keV isothermal collisionally-ionized emission model (CIE model in SPEX). The abundances of all the atomic species from carbon to iron were fixed to 0.65 similarly to the multiphase absorber.

We use these EPIC spectral fits to finally define a hybrid model which includes the nuclear emission (power law and Fe K line) intrinsically absorbed by the multiphase ICM plus the unabsorbed 1.5 arcmin cluster emission (CIE), both corrected by redshift and Galactic foreground. We simulate an *ASTRO-H*/SXS 100 ks exposure for two models with and without AGN intrinsic absorption. We could not distinguish between the models because the cluster accounts for more than 95 per cent of the emission within 1.5 arcmin. A very long exposure above 500 ks could potentially reveal some weak evidence of absorption. However, as previously mentioned, the AGN is brightening in recent years and at some point it may be as bright as in 1980, which was 10 times brighter than in 2006. We have therefore simulated a 500 ks *ASTRO-H*/SXS spectrum with three models of AGN absorption calculated for a combination of different velocity dispersion and line-of-sight velocity of the multiphase absorber (see Fig. 7). The lowest (blue) line in this figure includes a velocity offset of $-300\,\mathrm{km\,s^{-1}}$ (the bubble is likely rising buoyantly in the cluster potential) with a velocity dispersion of $300\,\mathrm{km\,s^{-1}}$ as a rough approximation of the expected velocity structure behind the weak shock along our line of sight (Fig. 6). The effects of absorption of the AGN are clearly noticeable.

Resonance line scattering of the emission from the ICM in the cluster is discussed in detail by Zhuravleva et al. (2013) and is not included in our modelling. We note that the largest red and

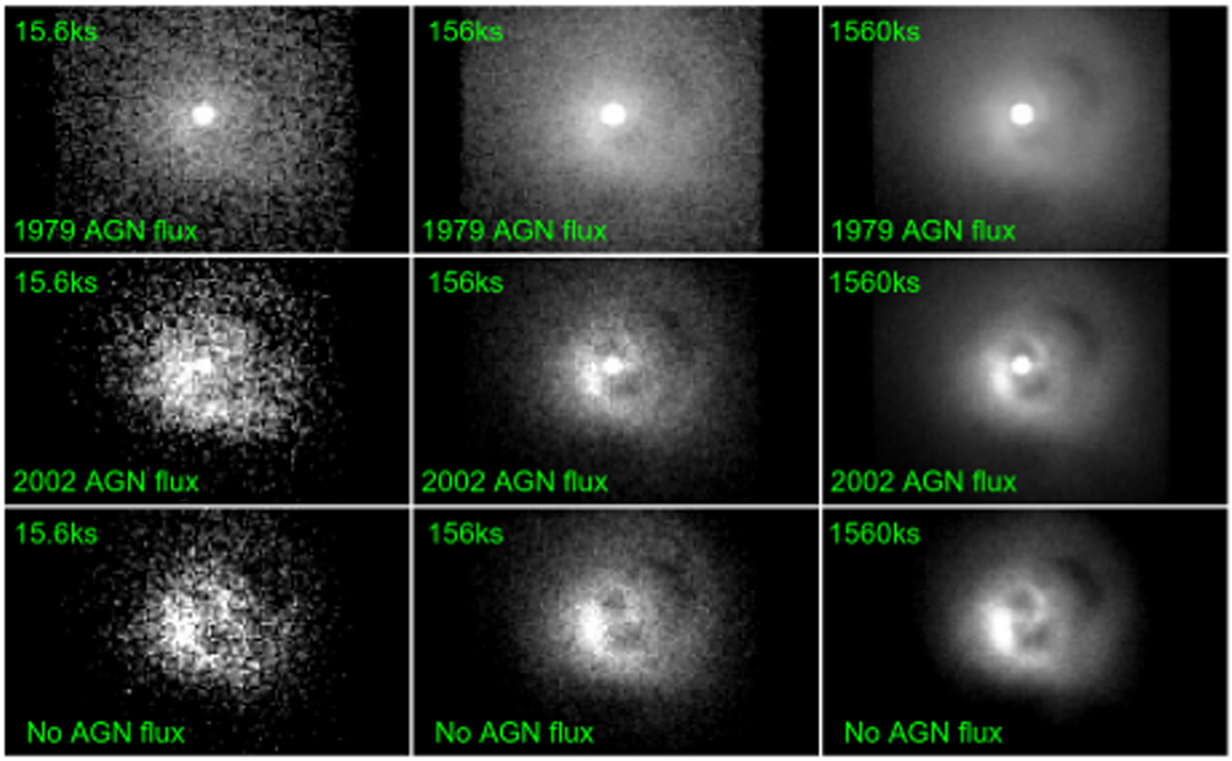

Figure 3. Simulated *Einstein* HRI images with different levels of central AGN X-ray flux and different exposure times (exposure times are 1×, 10× and 100× the 1979 *Einstein* observation exposure of 15.6 ks).

Table 2. Multiphase absorption model.

$T_{\rm range}$ (keV)	$T_{\rm adopted}$ (keV)	$N_{\rm H}(10^{21}$ cm$^{-2})$
<2.0	1.0	2.3
2.0–3.0	2.5	5.0
3.0–4.0	3.5	4.0
4.0–5.0	4.5	2.8
5.0–6.0	5.5	1.0

Notes. The model consists of five isothermal ionized absorber in collisional equilibrium, each of which has fixed temperature $T_{\rm adopted}$ and hydrogen column density $N_{\rm H}$.

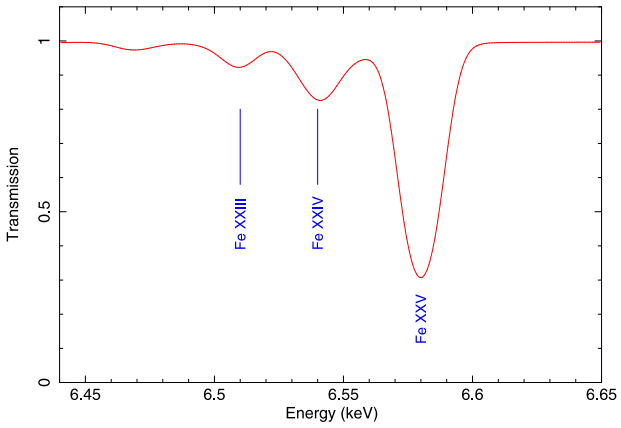

Figure 4. Transmission of the multiphase absorption model.

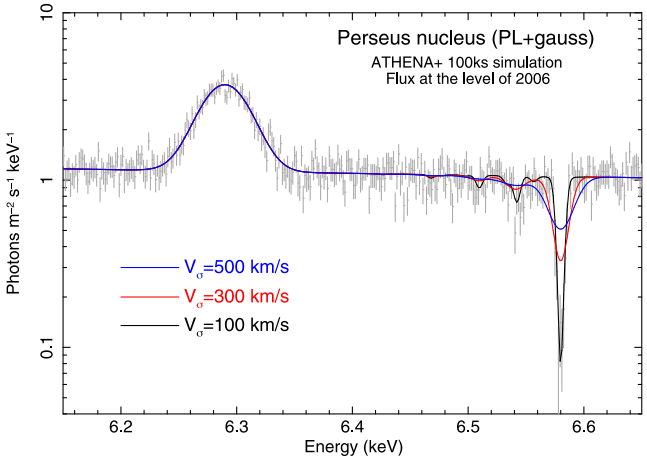

Figure 5. *Athena*/X-IFU simulation for the inner 14 arcsec.

blueshifted absorption components seen in the spectrum are likely to be due to the expanding inner bubbles.

We note that the shape of the 6.4-keV neural iron line (shown in Fig. 5) may hold interesting information (Churazov et al. 1998) about the velocity structure of the innermost massive molecular clouds surrounding the nucleus (Salomé et al. 2006; see also Jaffe 1990 for H I absorption against the nucleus).

5 DISCUSSION

We have shown that the X-ray bright nucleus can play both a negative and positive role in the detectability of features in the ICM. When the nucleus of NGC 1275 was very bright back in 1980 it prevented detection of the inner cavities. Our understanding of AGN

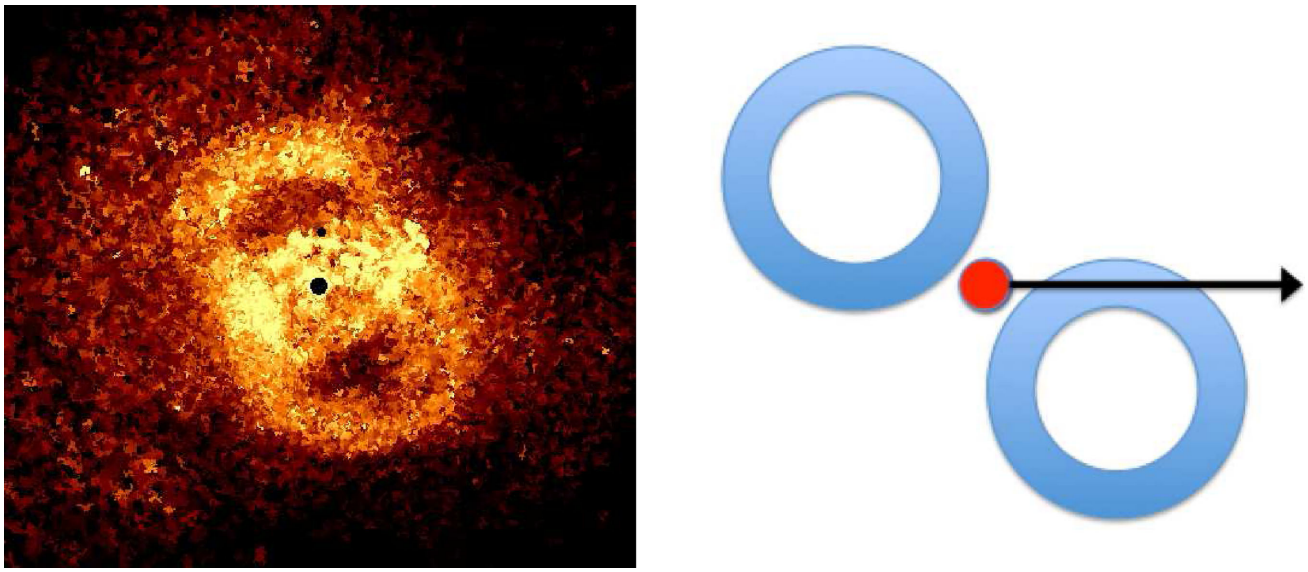

Figure 6. Left: pressure map of the region around NGC 1275. The bubbles are seen to be surrounded by spherical high pressure rings of shocked gas (see e.g. Graham et al. 2008). Right: schematic diagram showing how the bubbles probably lie along our line of sight, with the nucleus being viewed through the top part of the S bubble.

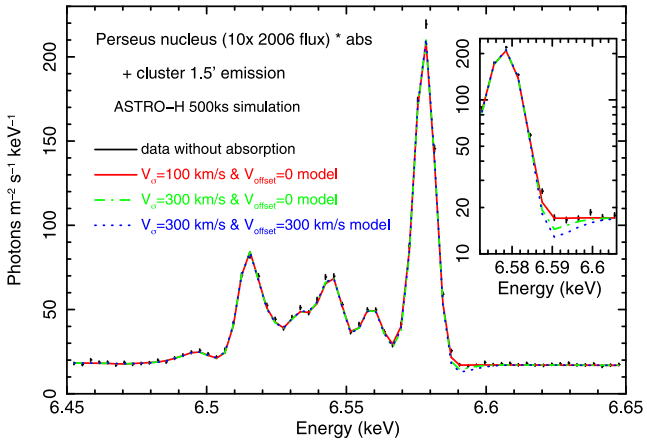

Figure 7. *ASTRO-H*/SXS simulation of the central 1.5-arcmin diameter cluster emission on top of an AGN spectrum 10 times brighter than in 2006. Three models of AGN instrinsic absorption are shown for a combination of different velocity dispersion and line-of-sight velocity.

feedback in clusters would have begun much earlier had the nucleus been weak at that time. If the nucleus brightens to a similar level in the next decade then it will enable unique absorption spectroscopy of the high pressure expanding rim around the inner southern cavity to be carried out.

Large variability of the jetted nucleus emission is common in cool core clusters. HST-1, part of the inner jet of M87, brightened and faded in X-rays by over an order of magnitude between 2004 and 2008 (Harris et al. 2009). Russell et al. (2013) find significant X-ray variability in the nucleus of A2052 and Hydra-A; Hogan et al. (2015) find high-frequency radio variability in 4 out of 23 central cluster sources. As shown above, an X-ray bright nucleus can enable X-ray absorption spectroscopy. The quasar H1821+643 at the centre of an X-ray luminous cluster at redshift $z - 0.297$ (Fang et al. 2002; Russell et al. 2010; Walker et al. 2014) is a potentially good target.

ACKNOWLEDGEMENTS

ACF, SAW and HRR acknowledge support from ERC AdG FEEDBACK. ACE acknowledges support from STFC grant ST/I001573/1.

REFERENCES

Abdo A. A. et al., 2009, ApJ, 699, 31
Allen S. W., Fabian A. C., Johnstone R. M., Edge A. C., Nulsen P. E. J., 1992, MNRAS, 254, 51
Boehringer H., Voges W., Fabian A. C., Edge A. C., Neumann D. M., 1993, MNRAS, 264, L25
Branduardi-Raymont G., Fabricant D., Feigelson E., Gorenstein P., Grindlay J., Soltan A., Zamorani G., 1981, ApJ, 248, 55
Churazov E., Sunyaev R., Gilfanov M., Forman W., Jones C., 1998, MNRAS, 297, 1274
Churazov E., Forman W., Jones C., Bohringer H., 2003, ApJ, 590, 225
Dutson K. L., Edge A. C., Hinton J. A., Hogan M. T., Gurwell M. A., Alston W. N., 2014, MNRAS, 442, 2048
Eyles C., Watt M. P., Bertram D., Church M. J., Ponman T. J., Skinner G. K., Willmore A. P., 1991, ApJ, 376, 23
Fabian A. C. et al., 1974, ApJ, 189, L59
Fabian A. C., Hu E. M., Cowie L. L., Grindlay J., 1981, ApJ, 248, 47
Fabian A. C. et al., 2000, MNRAS, 318, L65
Fabian A. C., Sanders J. S., Taylor G. B., Allen S. W., Crawford C. S., Johnstone R. M., Iwasawa K., 2006, MNRAS, 366, 417
Fang T., Davis David S., Lee Julia C. Marshall Herman L., Bryan Greg L., Canizares Claude R., 2002, ApJ, 565, 86
Graham J., Fabian A. C., Sanders J. S., 2008, MNRAS, 386, 278
Harris D. E., Cheung C. C., Stawarz L., Biretta J. A., Perlman E. S., 2009, ApJ, 699, 305
Hogan M. et al., 2015, MNRAS, in press
Jaffe W., 1990, A&A, 240, 254
Matt G. Costa E., dal Fiume D., Dusi W., Frontera F., Morelli E., 1990, ApJ, 255, 468
Osako C. Y. et al., 1994, ApJ, 435, 181
Primini F. A. et al., 1981, ApJ, 243, L13
Rothschild R., Baity W. A., Marscher A. P., Wheaton W. A., 1981, ApJ, 243, L9
Russell H. R., Sanders J. S., Fabian A. C., 2008, MNRAS, 390, 1207

Russell H. R., Fabian A. C., Sanders J. S., Johnstone R. M., Blundell K. M., Brandt W. N., Crawford C. S., 2010, MNRAS, 402, 1561
Russell H. R., McNamara B. R., Edge A. C., Hogan M. T., Main R. A., Vantyghem A. N., 2013, MNRAS, 432, 530
Salomé P. et al., 2006, A&A, 454, 437
Sanders J. S., Fabian A. C., 2007, MNRAS, 381, 1381
Ulmer M. P., Cruddace R. G., Fritz G. G., Snyder W. A., Fenimore E. E., 1987, ApJ, 319, 118
Van Speybroeck L. P., 1979, in Weisskopf M. C., ed., Proc SPIE Conf. Ser. Vol. 0184, Einstein Observatory (HEAO-B) Mirror Design and Performance. SPIE, Bellingham, p. 2
Walker S. A., Fabian A. C., Russell H. R., Sanders J. S., 2014, MNRAS, 442, 2809
Zhuravleva I. et al., 2013, MNRAS, 435, 3111

This paper has been typeset from a TEX/LATEX file prepared by the author.